Asian Journal of Chemistry; Vol. 35, No. 5 (2023), 1101-1109

ASIAN JOURNAL OF CHEMISTRY

https://doi.org/10.14233/ajchem.2023.27736

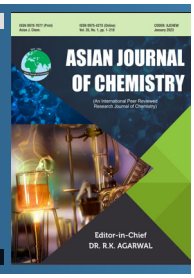

Highly Sensitive, Selective and Stable NO_2 Gas Sensor Based on Porous Influenced SnO_2 Bilayer Thin Films

R. YOGASARASWATHI* and J. DHEEPA

PG and Research Department in Physics, Government Arts College (Autonomous), Coimbatore-641018, India

*Corresponding author: E-mail: yogasaraswathi.astro@gmail.com

Received: 28 February 2023; *Accepted*: 30 March 2023; *Published online*: 28 April 2023; AJC-21216

In this work, an attempt has been made to fabricate SnO_2 porous films using automated nebulizer spray pyrolysis technique with the influence of a porogen. Pure tin dioxide and porous tin dioxide (SnO_2/SnO_2) thin films were prepared from a precursor solution composed of $SnCl_2{\cdot}2H_2O$ and polyethylene glycol as a porogen. The structural, morphological, optical and gas sensing performance of the prepared thin films were characterized. The inclusion of porogen significantly improved the sensing property of porous SnO_2 bilayer thin films and it was confirmed by structural, morphological and gas sensing performance studies. The optimized spray process parameter was determined finally in this work as SnO_2 precursor strength of 0.2 M for porous SnO_2 layer. Under this condition, the increased lattice constant, lattice defect and increased pores diameter were achieved, which exhibited good gas sensitivity and selectivity towards NO_2 gas at 250 ºC. The response and recovery time is decreased as 50%, the deduction limit is 0.9 ppm. In addition, during the five weeks test, the response level was observed nearly constant, which indicated that the SnO_2 bilayer sensor has long-term stability.

Keywords: Porous SnO_2, Bilayer films, Automated nebulizer spray technique, NO_2 gas sensor, Polyethylene glycol.

INTRODUCTION

Mostly gas sensors are fabricated from the metal oxide semiconductor (MOS) materials because of its electrical conductivity varies with various gas exposer and also has good sensing capacity, high reliability and good heat resistance [1]. This all characteristics are used to identify air pollutant gases like NO_2, NH_3, CO and gases that cause of global warming and among other things [2-4]. The changing resistivity is the basic phenomena of this metal oxide sensors, it is because of the intercommunication between sensor surface and injected gases finally the response decides whether it is highly sensitive or not. This technique is applied extensively in environmental monitoring system to deduct various dangerous and combustible gases and also in medical diagnosis apparatus, gas leakage indicators and food manufacturing. From last 10 years, interest of producing low-cost SnO_2 thin films are significantly increased. This is due to the attractive from scientific and technological curiosity in SnO_2 thin films with wide band gap n-type semi-conductors [5,6].

Tin oxide (SnO_2) thin films are fabricated from many techniques like sputtering [7], chemical vapour deposition [8], ion-beam assisted deposition [9], spray pyrolysis [10] and sol-gel techniques [11] are a few of them. Among these methods, spray pyrolysis has proven to be easy to use, repeatable, affordable and appropriate for applications involving a vast area. In addition to the straightforward experimental setup, their rapid growth rate and capacity for mass manufacturing of vast area coatings make them useful for industrial and many more applications. Additionally, spray pyrolysis makes it possible to regulate film shape and grain size in nanometer range [12].

Until date, nebulizer spray pyrolysis has been used by several researchers to create SnO_2. Considering the development of thin layers of SnO_2 [13], it is possible to manipulate the grain size in the film throughout a nanoscale range by adjusting the physical properties of the films like morphology, thickness and changing the deposition parameters like coating time, distance, hot plate temperature and annealing temperature [14]. SnO_2 pellets that have been partially sintered respond similarly [15, 16]. These marked the start of a quick phase of gas sensor development. Furthermore, a number of recent studies on the sensor characteristics of pure SnO_2 films near CO, NH_3, NO_2, H_2S and butane [17-21] seem to go toward the generally held opinion

that a high response can be expected, with the response being influenced by factors such as a porous surface and small grain size. The importance of fine grains and holes for the promised high sensitivity and fast response became evident in this way.

In this study, using an automated nebulizer spray pyrolysis method, porous SnO_2/SnO_2 thin films are prepared with porogen and their gas sensing properties are investigated.

EXPERIMENTAL

Tin chloride ($SnCl_2 \cdot 2H_2O$) was used to fabricate tin oxide films. A solvent solution of ethanol and double distilled water were mixed in the proportion ratio of 3:1. To achieve a desired precursor solution, exactly calculated amount of tin chloride was mixed with the solvent solution. Concentration of tin chloride was maintained as 0.3 M for pure SnO_2, while 0.1 M, 0.2 M and 0.3 M for porous SnO_2/SnO_2 thin films. The solution was then stirred in a magnetic stirrer until a clear precursor solution obtained. The glass substrate was placed on a hot platform preheated to 450 ºC and the precursor solution was sprayed onto it. The carrier gas pressure was kept constant at 0.5 bar. The spray nozzle was positioned at a 10 cm distance from the substrate. Throughout the experiment, the spray rate was kept constant at 0.1 mL/min, while the coating volume for pure SnO_2 was kept at 5 mL. To coat an additional porous tin oxide layer on pure tin oxide coated surface, tin chloride ($SnCl_2 \cdot 2H_2O$) and polyethylene glycol (PEG) were dissolved in 3:1 ratio distilled water and ethanol. PEG was added as a porogen [22,23] and the mixture was stirred well. After achieving the clear solution, it is transfer into the container and sprayed on pure SnO_2 layer and the coating volume is 1 mL for porous SnO_2 layers. After deposition, films were allowed to cool at an ambient temperature [24-26].

RESULTS AND DISCUSSION

X-ray diffraction studies: Structural properties of the films were studied using XRD pattern (Fig. 1). The obtained peaks were compared with JCPDS cards and all the peaks were well matched at an angle 2θ = 26.6º, 33.89º and 51.78º. The polycrystalline tetragonal rutile-type SnO_2 phase occurs in all the cases and the peak positions of all the films correlate well with JCPDS card no. 41-1445. It should be observed that the position of the SnO_2 peaks were unchanged but the intensity is decreased due to the presence of porous surface layer. Porous SnO_2/SnO_2 film prepared from 0.2 M concentration exhibits the highest intensity than other porous bilayer films.

The grain size was found to be in the range of several nanometers the calculated grain size is shown in Table-1, the FWHM

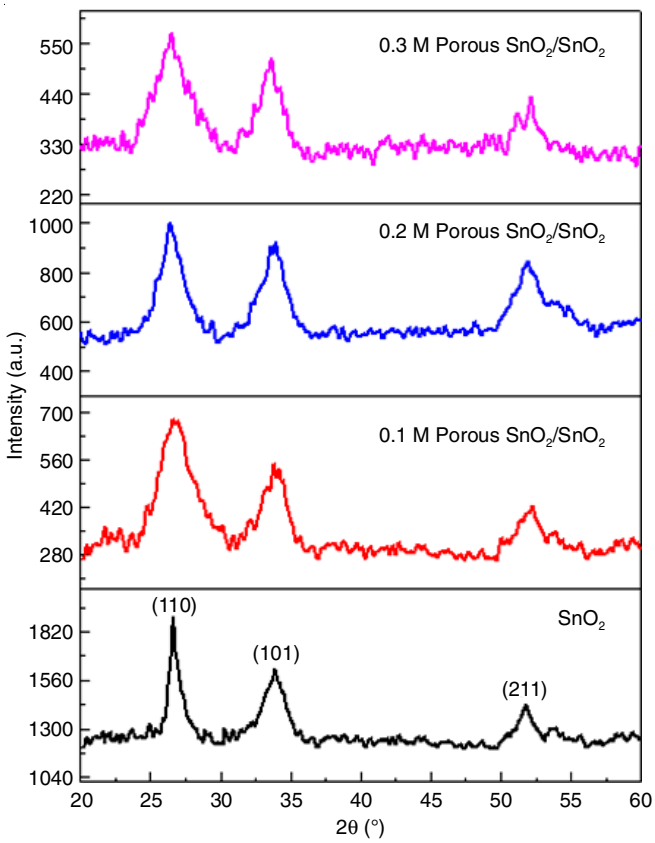

Fig. 1. XRD pattern for pure SnO_2 and porous SnO_2/SnO_2 thin films at different concentrations

of the diffracted peak was used to determine strain and grain size. Eqns. 1 and 2 were used to obtain the average grain size (D) and lattice constants [27]:

$$D = \frac{k\lambda}{\beta \cos\theta} \quad (1)$$

$$\frac{1}{d^2} = \frac{h^2 + k^2}{a^2} + \frac{l^2}{c^2} \quad (2)$$

where λ = X-ray wavelength, θ = Bragg's diffracted angle, β = full width at half maximum (FWHM) and d = inter-planar spacing. Based on this equation, the grain size is in the range of nanometers.

The lattice strain (ε) and dislocation density (δ) of the SnO_2 and porous SnO_2 bilayer thin films can be obtained from eqn. 3 and 4 [28,29]. Table-1 depicts the values of the calculated microstructural parameters, it shows a randomly varied grain size, dislocation density and strain for pure SnO_2 films and different concentrated porous SnO_2/SnO_2 films. In order to

TABLE-1
CALCULATED STRUCTURAL PARAMETERS OF PURE SnO_2 AND POROUS SnO_2/SnO_2 THIN FILMS

Sample	Lattice constant (Å)		Film thickness (μm)	Grain size (nm)	Dislocation density ($\times 10^{15}$) lines (m^{-2})	Micro strain ($\times 10^{-3}$)
	a	c				
SnO_2	4.7031	3.1733	119. 50	56.66	0.312	20.21
0.1 M Porous SnO_2/SnO_2	4.5931	3.1341	212.92	32.72	0.934	35.71
0.2 M Porous SnO_2/SnO_2	4.6184	3.1393	213.22	33.72	0.879	32.22
0.3 M Porous SnO_2/SnO_2	4.5573	3.1327	213	34.37	0.846	31.06

improve sensing performance, increasing tin chloride content in the porous layer increases the number of defects [30].

$$\varepsilon = \frac{\beta}{4\tan\theta} \quad (3)$$

$$\delta = \frac{1}{D^2} \quad (4)$$

The obtained grain size D was in the range of 56.66 nm for pure SnO_2 and 32.72 nm, 33.72 nm and 34.37 nm for porous SnO_2/SnO_2 films at different concentration of 0.1, 0.2 and 0.3 M, respectively. Due to the pores formation, in porous SnO_2/SnO_2 film a grains become very smaller than pure SnO_2 film. The c/a ratio for pure SnO_2 and porous SnO_2/SnO_2 films which was found to be decreased. Comparing to other porous SnO_2 bilayer, porous SnO_2/SnO_2 film prepared with 0.2 M concentration exhibits the higher lattice constant and shows that the lattice in axis-*a* has expanded. This expanded lattice constant and increase in lattice defect may improve gas sensing performance [30].

Elemental analysis: EDAX spectrum were used to examine the elemental analysis of the prepared films (Fig. 2). The weight % for the EDAX are provided in the table inset of Fig. 2. Tin, oxide and silicon were present in both SnO_2 films and porous SnO_2/SnO_2 films. The Sn and O content increases with weight percentage in porous SnO_2/SnO_2 films due to the additional porous SnO_2 layer coated on pure SnO_2 film.

Morphological studies: Pure SnO_2 and porous SnO_2/SnO_2 thin films (Fig. 3) depicts the surface microstructure of the prepared SnO_2 based bilayer thin film as studied by FESEM. The result shows that the flower like structure appeared in pure SnO_2 film (Fig. 3a) and the formation of porous surface in SnO_2 layer was confirmed (Fig. 3b-d). On the whole surface of porous SnO_2/SnO_2 films exhibits very small nanoporous structures. Besides, the arrangement and size of the pores appears to be uneven. It has been observed that porous SnO_2/SnO_2 films have small, spherical, spongy clusters made up of a large number of randomly arranged nanoparticles. There is observable difference occurred between pure SnO_2 and porous SnO_2/SnO_2 films. By direct measurement from FESEM image of porous layer, the porous diameter is measured. The average pores size is 192.61 nm, 239.71 nm and 151.21 nm belong to different concentration of 0.1, 0.2 and 0.3 M, respectively. From Table-1, the grain size of porous SnO_2 layer was found to be increases with increasing the concen-tration of precursor. It can be explained by Ostwald ripening [31,32]. And also, at higher concentration (0.3 M) it seems to have more combined SnO_2 particle to cover the pores [32,33]. So the porous diameter is decreased, which is due to the increase of grain size in porous SnO_2 layer. At lower concentrations (0.1 M and 0.2 M), nanoparticle size and porous size are in good argument.

Optical characterization

UV-vis studies: The UV-vis spectrum between 200 to 800 nm were used to investigate the optical characteristics of the fabricated films. The optical absorption spectra of the deposited films are shown in Fig. 4. According to the obtained spectrum, absorbance was increased with increasing wavelength above 250 nm. The wavelength with the maximum absorption was 318 nm for pure SnO_2 and 304 nm for porous SnO_2/SnO_2 thin film.

Using the correlation between absorbance and photon energy, the optical band gap (E_g) was calculated [28]. The optical absorption coefficient α at the absorption edge for direct allowed transitions is given by eqn. 5:

$$(\alpha h\nu)^2 = A\,(h\nu - E_g) \quad (5)$$

where A = absorption constant for a direct transition, h = Planck's constant, ν = photon frequency and E_g = optical band gap.

The band gap for a direct allowed transition can be estimated by plotting $(\alpha h\nu)^2$ *vs.* $h\nu$ (Fig. 5). The obtained band gap value of deposited films are 3.44 eV for pure SnO_2 and 3.70 eV, 3.58 eV and 3.75 eV for porous SnO_2/SnO_2 films with 0.1, 0.2 and 0.3 M, respectively. The band gap value found to be higher for porous SnO_2/SnO_2 films than pure SnO_2 film, it is due to the decrease in particle size and increase in the film thickness by adding an additional layer of porous SnO_2 on pure SnO_2 thin film. In Fig. 5b, porous SnO_2/SnO_2 film deposited using 0.2 M concentration exhibits lower band gap value than other concentration of porous SnO_2/SnO_2 films, it may be due to an increases of grain size, lattice constant and porous diameter.

Photoluminescence studies: Photoluminescence (PL) spectra of pure SnO_2 and porous SnO_2/SnO_2 films at emission wavelength over 300 nm are shown in Fig. 6. The highest emission intensity peak were observed at 392 nm for pure SnO_2 film and 381 nm for porous SnO_2/SnO_2 films. With the addition of porogen, the peak emission intensity were decreased and there was a significant shift towards a lower wavelength at

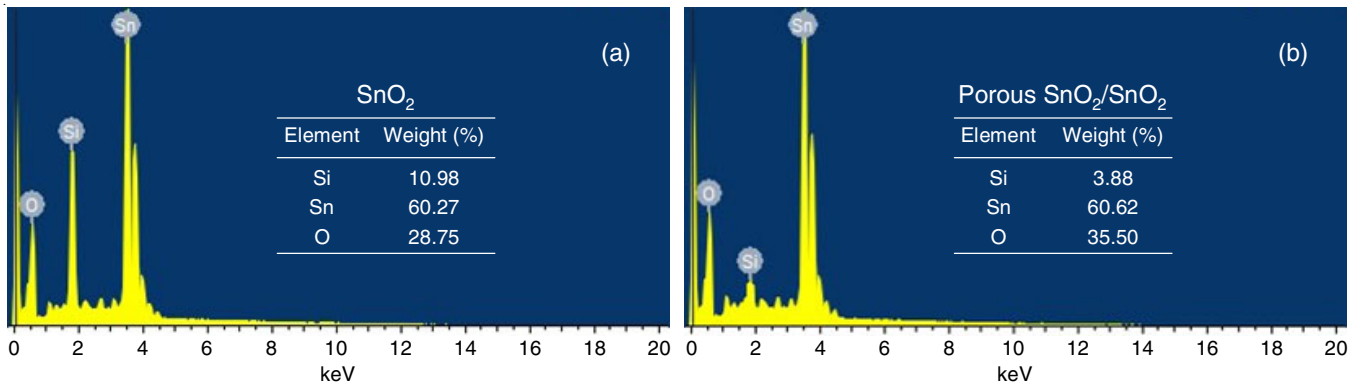

Fig. 2. EDAX spectra of (a) Pure SnO_2, and (b) Porous SnO_2/SnO_2 thin films

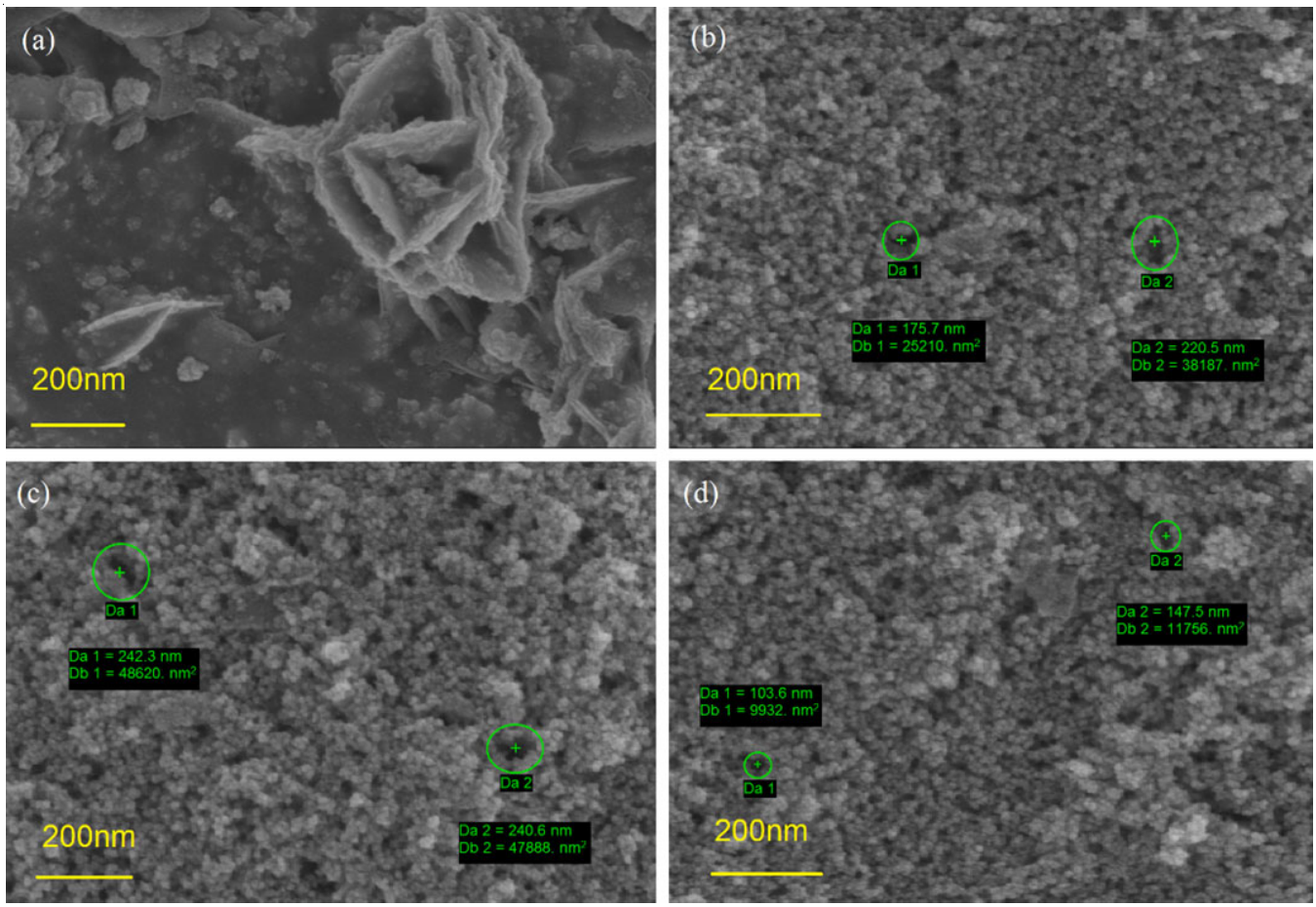

Fig. 3. Surface morphology of (a) SnO_2, (b) 0.1 M, (c) 0.2 M and (d) 0.3 M of porous SnO_2/SnO_2 thin films

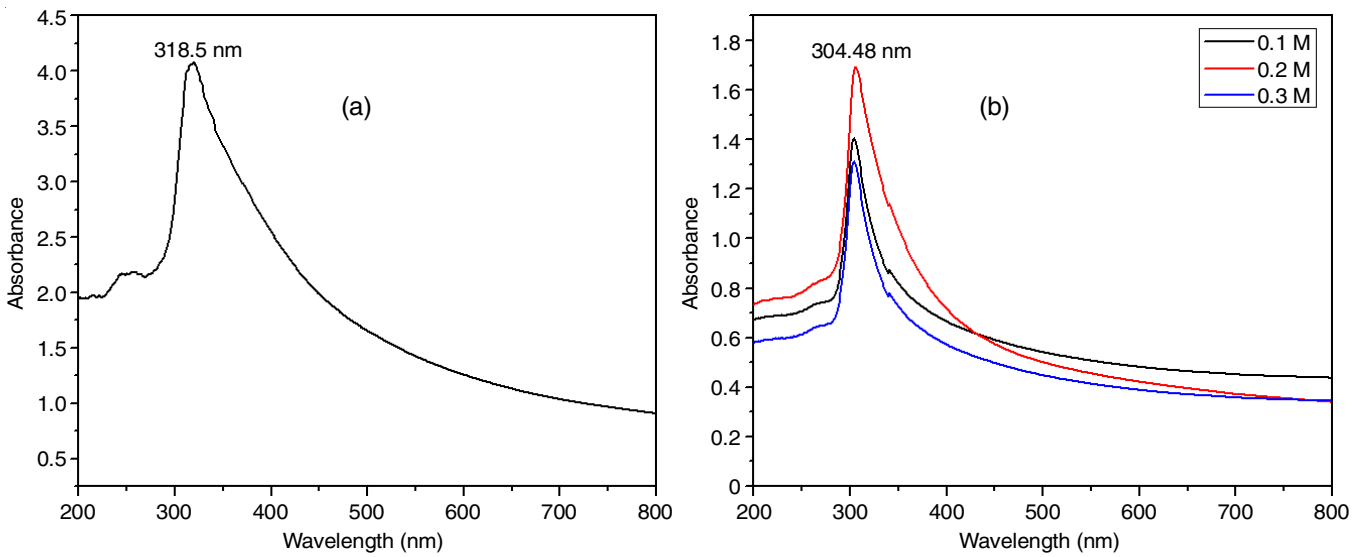

Fig. 4. UV-visible spectroscopy of (a) SnO_2 film, (b) porous SnO_2/SnO_2 thin films at different concentrations

porous SnO_2 bilayer films. Pores that produce lattice defects, were a major reason to this shift [34,35].

Electrical measurements: The ohmic contact of the prepared films were measured by current-voltage characteristics (I-V). Since the Schottky barrier formation is minimal, the outcome as shown in Fig. 7 is a linear correlation of the polarized voltage. The films conduct current in both negative and positive direction with small resistance value for pure SnO_2 film and large resistance value for porous SnO_2 bilayer films. This may be for the reason of microstructure played a main role as comparing to porous SnO_2/SnO_2 films, pure SnO_2 film allowed electrons overcome the barrier with low resistivity, due to its plain and smooth surface. So that, IV characteristics of pure SnO_2 plot shows small resistance curve than porous SnO_2/SnO_2 film.

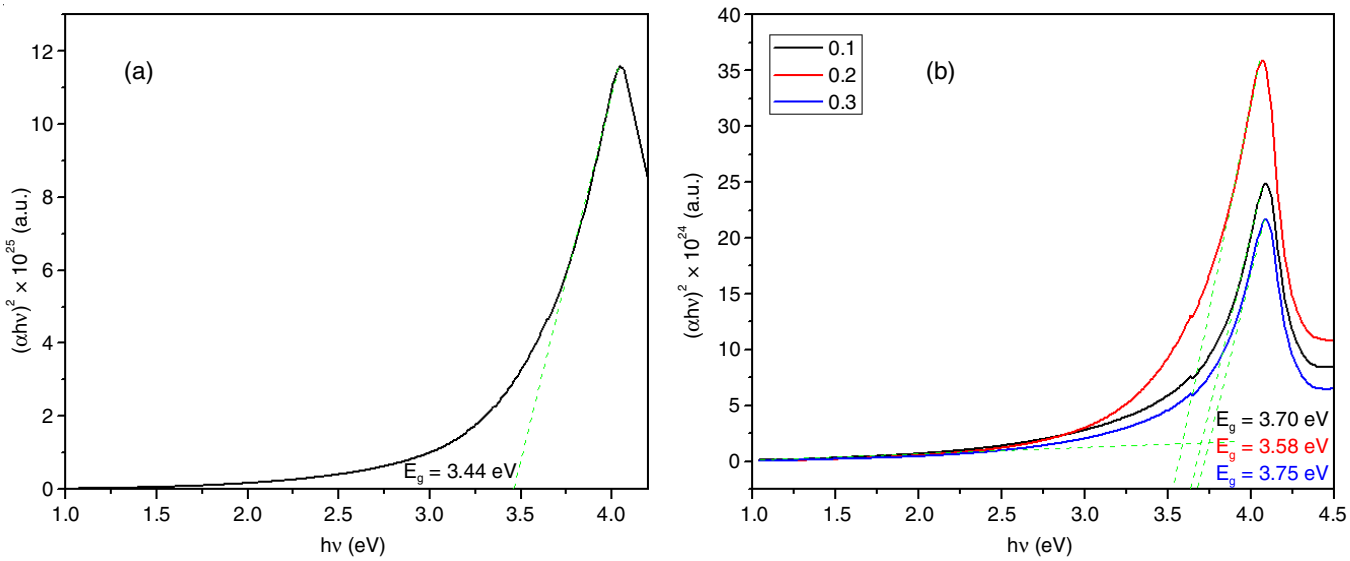

Fig. 5. Plot of $(\alpha h\nu)^2$ *vs*. photon energy (hν) for (a) pure SnO_2 film and (b) porous SnO_2/SnO_2 thin films at different concentrations

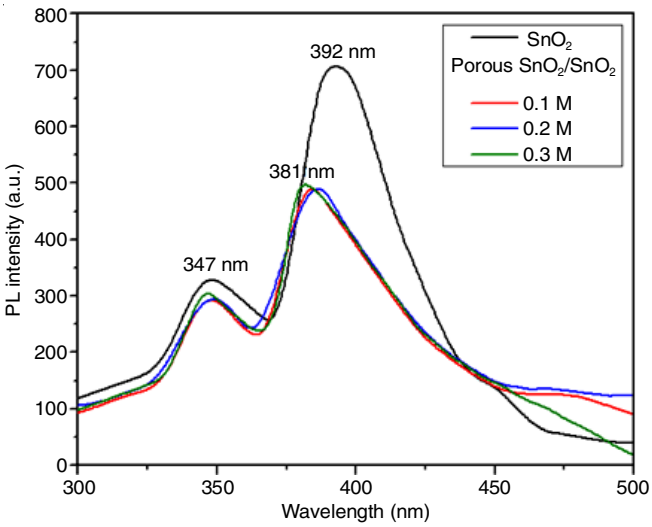

Fig. 6. Photoluminescence (PL) emission spectrum of SnO_2 and porous SnO_2 bilayer thin films at different concentrations

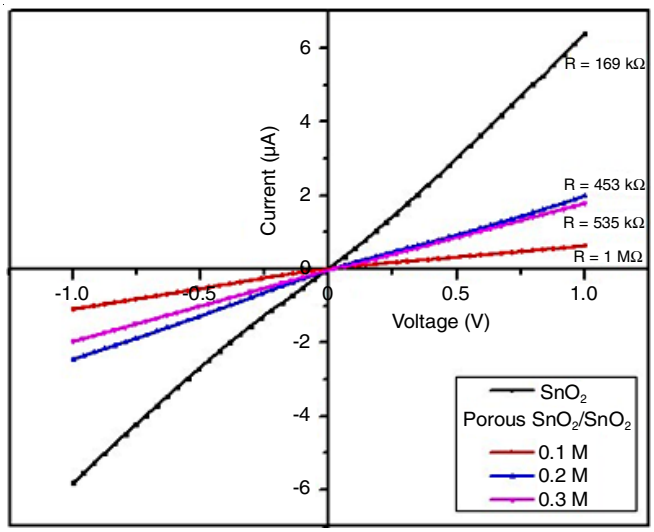

Fig. 7. IV characteristics of SnO_2 and porous SnO_2 bilayer thin films at different concentrations

Generally, the conductivity of the sample is expected to reduce with the presence of pores and this depends on the proportion of porosity [36,37].

Gas sensing measurements: The dynamic gas sensing arrangement was used to test the gas sensing properties of SnO_2 and porous SnO_2/SnO_2 thin films by using different types of reducing and oxidizing gases at various working temperatures and gas concentrations. The response of the sample towards the operating gas was determined by molarity of main material, film thickness, surface morphology, oxygen vacancies, grain size, nature of the gas and operating temperatures [38].

The prepared thin film samples were tested in 50 ppm to 400 ppm gas concentration of CO, NH_3 and NO_2 gases at working temperature of room temperature to 250 ºC. Fig. 8 depicts the response chart of different gases performed in different operating temperature (Fig. 8a) and various gas concentration (Fig. 8b). All SnO_2 samples are shown to respond most strongly at 250 ºC, and the thin sheet made from a porous SnO_2/SnO_2 precursor at a strength of 0.2 M is the most sensitive to NO_2 gas at 100 ppm. Besides, pure SnO_2 and 0.2 M porous SnO_2/SnO_2 films with increasing gas concentrations shows increasing response towards NH_3 and NO_2 gases at 250 ºC.

Fig. 9 shows the real-time dynamic resistance response of as-deposited SnO_2 sample and optimized porous SnO_2 bilayer sample, it is comparison of both films responding for NH_3 and NO_2 gases. It was observed that 0.2 M strength porous SnO_2/SnO_2 film shows the highest response towards NO_2 gas. However, for porous SnO_2/SnO_2 thin films with increasing gas concentrations shows incredible response towards NO_2 gas is observed at 250 ºC working temperature (Fig. 9d), the resistivity of the film increases from kilo ohm (kΩ) to mega ohm (MΩ) so it is evident that porous SnO_2/SnO_2 film shows high response towards NO_2 gas than pure SnO_2 thin film.

The selectivity of the fabricated SnO_2 based thin films were measured towards various gases and corresponding graph is plotted in Fig. 10. It is observed that NO_2 gas response is higher for porous SnO_2 bilayer and is very less for all other gases,

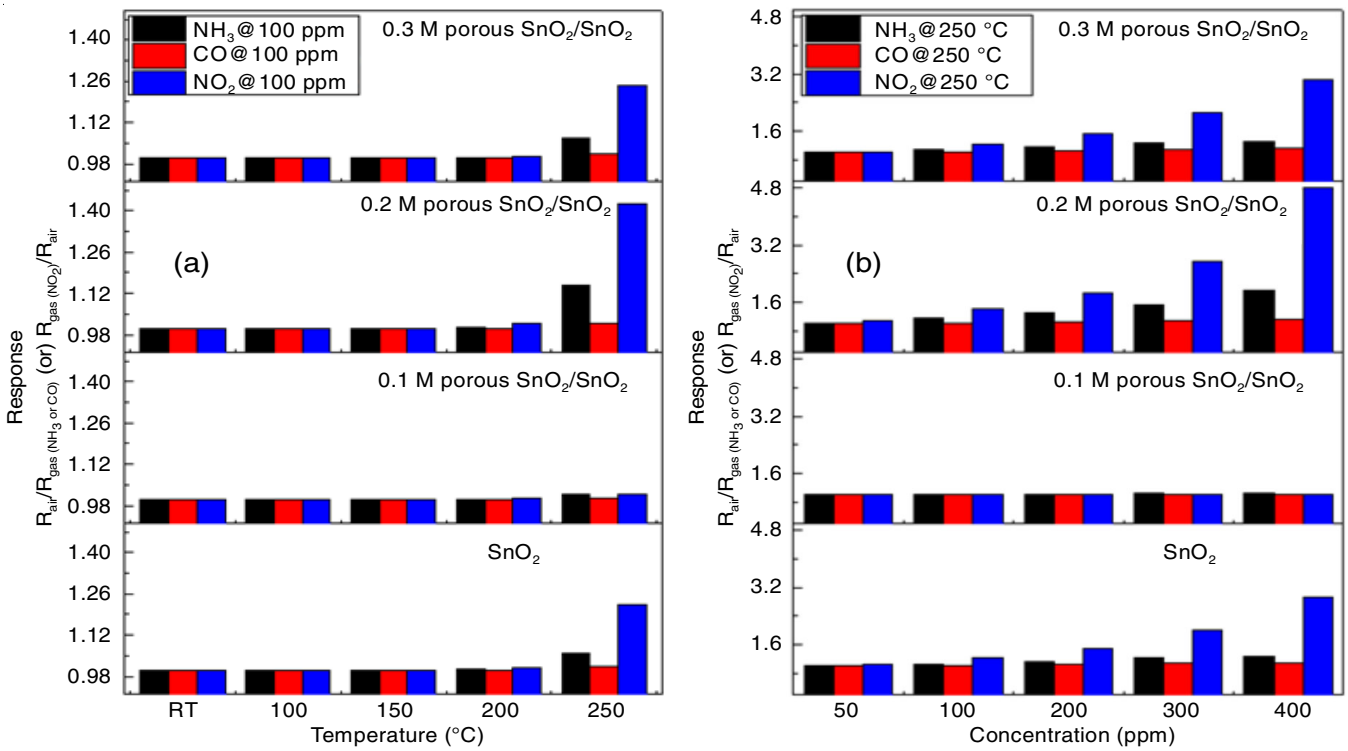

Fig. 8. Gas response bar chart at different temperature (a) and various gas concentration (b) of pure SnO_2 thin film and porous SnO_2/SnO_2 thin films with different molarity

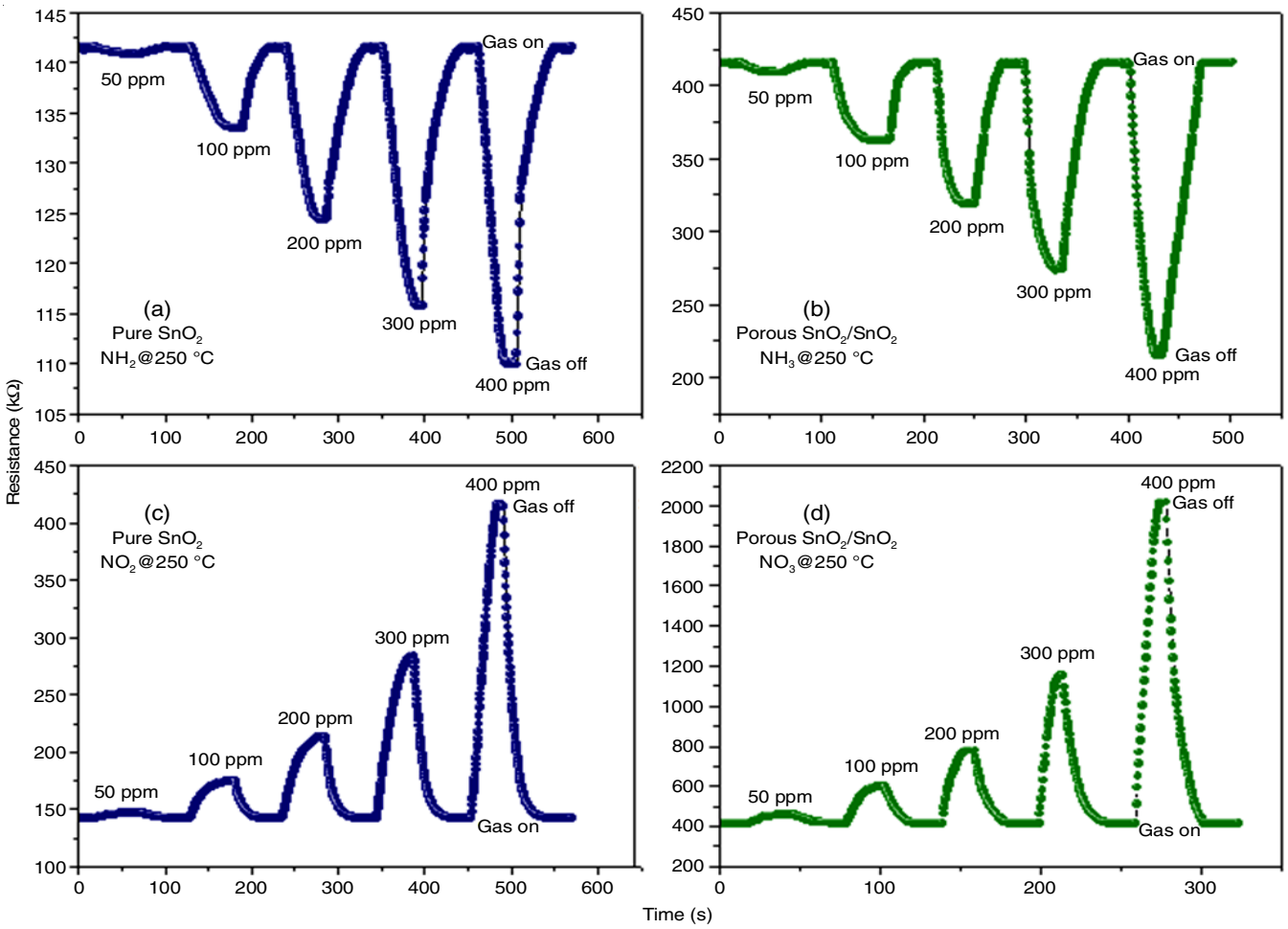

Fig. 9. Dynamic gas response of (a), (c) pure SnO_2 and (b), (d) 0.2 M porous SnO_2/SnO_2 thin films

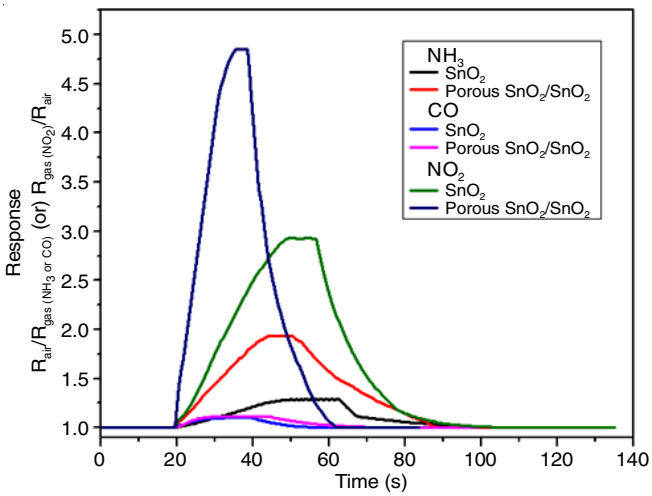

Fig. 10. Selectivity graph of prepared thin films towards different gases at 400 ppm and 250 ºC

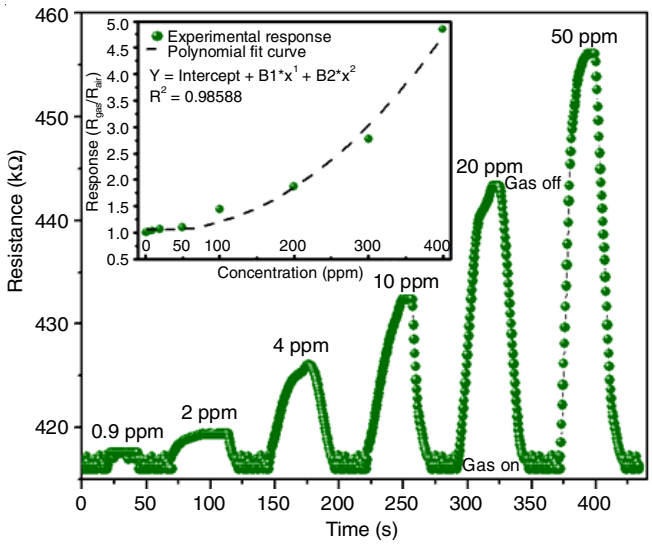

Fig. 12. Dynamic gas response of porous SnO_2 bilayer sensor at minimum NO_2 gas concentration (Inset: curve fitting of experimental response)

so it confirms porous SnO_2 bilayer was exclusively selective for NO_2 gas.

Response and recovery time: Fig. 11a-b depicts the response and recovery time of pure SnO_2 and porous SnO_2/SnO_2 thin films for 400 ppm NO_2 gas at 250 ºC. Porous SnO_2/SnO_2 film reaches its maximum reaction time of 12 s and recovers in 23 s. When compared to unadulterated SnO_2 film, it is obviously lower. This suggests that the porous SnO_2/SnO_2 film has an ability to function as a sensitive material, with a fast response and recovery period. Therefore, extensive gas sensing study is conducted on this specific composition.

Limit of deduction: Limit of deduction is further investigated of minimum concentration of NO_2 gas from 0 to 50 ppm. From Fig. 12, porous SnO_2/SnO_2 film can detect NO_2 gas at a very less concentration of 0.9 ppm. The curve fitting of the response (inset, Fig. 12), it is observed non-linear polynomial dependence of response towards NO_2 gas concentration in the range with a non-linear correlation coefficient (R^2) of 0.985.

Long-term stabilities: Long-term stability is one of the important parameter for gas sensor. So that it was tested upto 35 days on same porous SnO_2 bilayer sample towards 50 ppm of NO_2 gas as shown in Fig. 13. It was observed that almost unchanged response for 5 weeks in 250 ºC, the formation of oxidation causes a very small change in the response. Besides, porous SnO_2 bilayer sensor seems good long-term stability so as a result, it is used to detect very sensitive and selective NO_2 gas with low concentrations and good long-term stability.

Previously reported articles deals the fabrication of porous surface for gas sensor application by using etching, laser ablation, frame work, membrane, polymer, self-assembling, spin coating methods, sputtering, *etc.* [39-44]. Herein, we reported fabricating porous surface by using PEG in automated nebulizer spray pyrolysis method. This porogen PEG is used in many methods to fabricate pores, especially in spin coating [22,23] from this field it is very rare to fabricate porous surface in the method of automated nebulizer spray pyrolysis (ANSP) by using PEG. The prepared sample was performed well towards NO_2 gas, it shows comparatively equal response of other porous thin films.

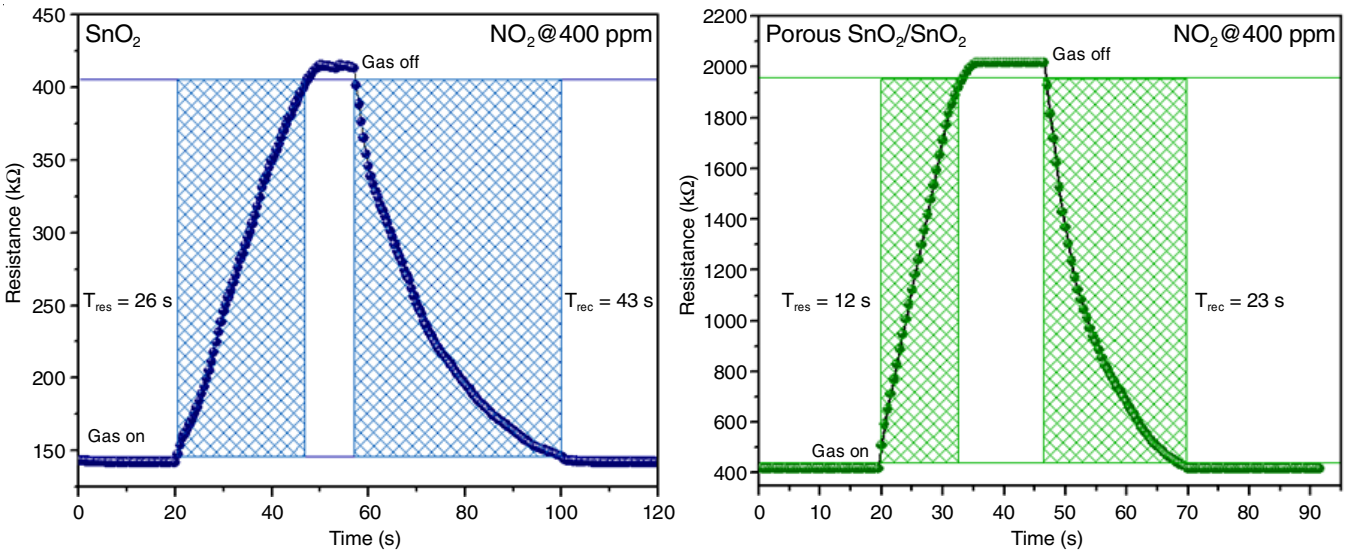

Fig. 11. Response and recovery time of pure SnO_2 and porous SnO_2/SnO_2 thin film of NO_2 at 250 ºC

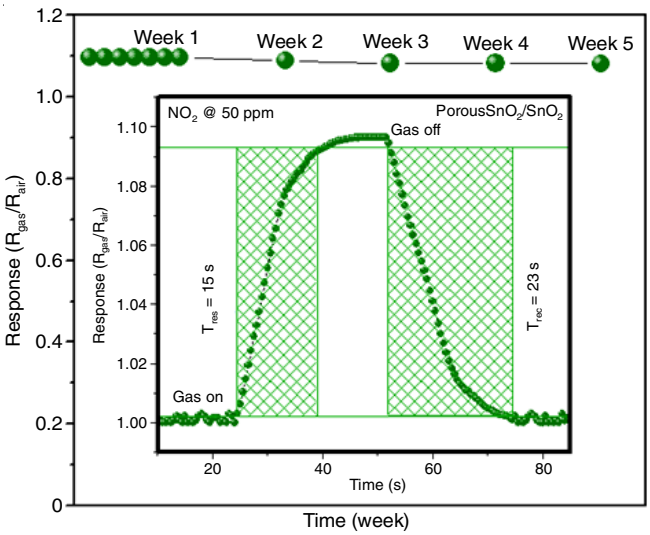

Fig. 13. Long-term response of porous SnO_2 bilayer sensor towards 50 ppm of NO_2 at 250 ºC (Inset: response and recovery time of the sample in 5th week)

Conclusion

Tin oxide based thin films were fabricated successfully by automated nebulizer spray pyrolysis (ANSP) technique. The XRD, EDAX, FESEM, UV-visible, photoluminescence, IV characteristic and gas sensor performance were used to analyze the prepared thin films. The XRD pattern revealed the structural properties of prepared samples, the calculated grain size seems to be decreased at an impact of porosity. The surface morphology confirms the presence of porous in corresponding thin films.The IV characteristic graph showed the super linear resistance behaviour. A complete gas sensing behaviour of the films were analyzed by dynamic method. It reveals that porous SnO_2 bilayer sensor is highly sensitive and selective towards NO_2 gas and also has good sensing performance at minimum gas concentration of 0.9 ppm. Long-term stability of the sensor is demonstrated by its virtually constant response over a period of about 5 weeks of data. Thus, it can be assumed that the porous SnO_2/SnO_2 thin film fabricated by the precursor strength of 0.2 M has the potential to be an effective NO_2 gas sensor.

CONFLICT OF INTEREST

The authors declare that there is no conflict of interests regarding the publication of this article.

REFERENCES

1. B. Saruhan, R.L. Fomekong and S. Nahirniak, *Front. Sens.*, **2**, 657931 (2021); https://doi.org/10.3389/fsens.2021.657931
2. A. Ponzoni, C. Baratto, N. Cattabiani, M. Falasconi, V. Galstyan, E. Nunez-Carmona, F. Rigoni, V. Sberveglieri, G. Zambotti and D. Zappa, *Sensors*, **17**, 714 (2017); https://doi.org/10.3390/s17040714
3. C. Wang, L. Yin, L. Zhang, D. Xiang and R. Gao, *Sensors*, **10**, 2088 (2010); https://doi.org/10.3390/s100302088
4. G,F. Fine, L.M. Cavanagh, A. Afonja and R. Binions, *Sensors*, **10**, 5469 (2010); https://doi.org/10.3390/s100605469
5. O. Mounkachi, E. Salmani, M. Lakhal, H. Ez-Zahraouy, M. Hamedoun, M. Benaissa, A. Kara, A. Ennaoui and A. Benyoussef, *Solar Energy Mater. Solar Cells*, **148**, 34 (2016); https://doi.org/10.1016/j.solmat.2015.09.062
6. A.L. Resne and Z. Tariq, *IOP Conf. Ser.: Mater. Sci. Eng.*, **571**, 012105 (2019); https://doi.org/10.1088/1757-899X/571/1/012105
7. E. Turan, M. Kul and S. Akin, *J. Mater. Sci. Mater. Electron.*, **33**, 15689 (2022); https://doi.org/10.1007/s10854-022-08472-7
8. N. Najafi and S.M. Rozati, *Acta Phys. Pol. A*, **131**, 222 (2017); https://doi.org/10.12693/APhysPolA.131.222
9. B.-K. Min and S.-D. Choi, *Sens. Actuators B Chem.*, **98**, 239 (2004); https://doi.org/10.1016/j.snb.2003.10.023
10. D. Leng, L. Wu, H. Jiang, Yu. Zhao, J. Zhang, W. Li and L. Feng, *Int. J. Photoenergy*, **2012**, 235971 (2012); https://doi.org/10.1155/2012/235971
11. M. Marikkannan, V. Vishnukanthan, A. Vijayshankar, J. Mayandi and J.M. Pearce, *AIP Adv.*, **5**, 027122 (2015); https://doi.org/10.1063/1.4909542
12. L.A. Patil, D.N. Suryawanshi, I.G. Pathan and D.G. Patil, *Bull. Mater. Sci.*, **37**, 425 (2014).
13. J. Sundqvist, J. Lu, M. Ottosson and A. Hårsta, *Thin Solid Films*, **514**, 63 (2006); https://doi.org/10.1016/j.tsf.2006.02.031
14. G. Korotcenkov, M. DiBattista, J. Schwank and V. Brinzari, *Mater. Sci. Eng. B*, **77**, 33 (2000); https://doi.org/10.1016/S0921-5107(00)00455-4
15. G.E. Patil, D.D. Kajale, D.N. Chavan, N.K. Pawar, P.T. Ahire, S.D. Shinde, V.B. Gaikwad and G.H. Jain, *Bull. Mater. Sci*., **34**, 1 (2011).
16. K. Nomura, H. Shiozawa, T. Takada, H. Reuther and E. Richter, *J. Mater. Sci. Mater. Electron.*, **8**, 301 (1997); https://doi.org/10.1023/A:1018535322380
17. A.K. Gangwar, R. Godiwal, S. Srivastava, P. Pal, G. Gupta and P. Singh, *Mater. Res. Bull.*, **148**, 111692 (2022); https://doi.org/10.1016/j.materresbull.2021.111692
18. J. Rzaij, A. Khalil and S. Nawaf, *World J. Adv. Res. Revs.*, **14**, 051 (2022); https://doi.org/10.30574/wjarr.2022.14.1.0288
19. Y. Yang, B. Maeng, D.G. Jung, J. Lee, Y. Kim, J.B. Kwon, H.K. An and D. Jung, *Nanomaterials*, **12**, 3227 (2022); https://doi.org/10.3390/nano12183227
20. U.D. Lad, N.S. Kokode and U.J. Tupe, *Adv. Mat. Res.*, **1172**, 67 (2022); https://doi.org/10.4028/p-2zz6i6
21. M.A. Han, H.-J. Kim, H.C. Lee, J.-S. Park and H.-N. Lee, *Appl. Surf. Sci.*, **481**, 133 (2019); https://doi.org/10.1016/j.apsusc.2019.03.043
22. S.J. Bu, Z.G. Jin, X.X. Liu, L.R. Yang and Z.J. Cheng, *J. Eur. Ceram. Soc.*, **25**, 673 (2005); https://doi.org/10.1016/j.jeurceramsoc.2003.12.025
23. P. Zhou, Y. Shen, S. Zhao, G. Li, Y. Yin, R. Lu, S. Gao, C. Han and D. Wei, *J. Alloys Compd.*, **789**, 129 (2019); https://doi.org/10.1016/j.jallcom.2019.03.038
24. S. Palanichamy, J. Raj Mohamed, K. Deva Arun Kumar, P.S. Satheesh Kumar, S. Pandiarajan and L. Amalraj, *Optik*, **194**, 162887 (2019); https://doi.org/10.1016/j.ijleo.2019.05.093
25. R. Mariappan, V. Ponnuswamy, P. Suresh, R. Suresh, M. Ragavendar and C. Sankar, *Mater. Sci. Semicond. Process.*, **16**, 825 (2013); https://doi.org/10.1016/j.mssp.2013.01.006
26. K.D.A. Kumar, S. Valanarasu, K. Jeyadheepan, H.-S. Kim and D. Vikraman, *J. Mater. Sci. Mater. Electron.*, **29**, 3648 (2018); https://doi.org/10.1007/s10854-017-8295-2
27. Z. Hajizadeh, R. Taheri-Ledari and F.R. Asl, Micro and Nano Technologies, Heterogeneous Micro and Nanoscale Composites for the Catalysis of Organic Reactions, Elsevier, pp. 33-51 (2022).
28. V.S. Vinila and J. Isac, eds.: S. Thomas, N. Kalarikkal and A.R. Abraham, Synthesis and Structural Studies of Superconducting Perovskite $GdBa_2Ca_3Cu_4O_{10.5+\delta}$ Nanosystems, In: Micro and Nano Technologies, Design, Fabrication and Characterization of Multifunctional Nanomaterials, Elsevier, pp. 319-341 (2022).
29. N.D. Mohd Said, M.Z. Sahdan, N. Nayan, H. Saim, F. Adriyanto, A.S. Bakri and M. Morsin, *RSC Adv.*, **8**, 29686 (2018); https://doi.org/10.1039/C8RA03950J

30. S. Maheswari, M. Karunakaran, K. Kasirajan, L. Bruno Chandrasekar and P. Boomi, *Sens. Actuators A Phys.*, **315**, 112303 (2020); https://doi.org/10.1016/j.sna.2020.112303
31. G. Singh, S.B. Shrivastava, D. Jain, S. Pandya and V. Ganesan, *Defect and Diffusion Forum*, **293**, 99 (2009); https://doi.org/10.4028/www.scientific.net/DDF.293.99
32. K.A. Eswar, A.A. Azlinda, F.S. Husairi, M. Rusop and S. Abdullah, *Adv. Mater. Res.*, **701**, 167 (2013); https://doi.org/10.4028/www.scientific.net/AMR.701.167
33. M. Wang, J. Wang, W. Chen, Y. Cui and L. Wang, *Mater. Chem. Phys.*, **97**, 219 (2006); https://doi.org/10.1016/j.matchemphys.2005.07.072
34. X. Wu, Z. Wei, L. Zhang, X. Wang, H. Yang and J. Jiang, *J. Nanomater.*, **2014**, 792102 (2014); https://doi.org/10.1155/2014/792102
35. C.M. Liu, X.T. Zu, Q.M. Wei and L.M. Wang, *J. Phys. D Appl. Phys.*, **39**, 2494 (2006); https://doi.org/10.1088/0022-3727/39/12/004
36. F. Ternero, L.G. Rosa, P. Urban, J.M. Montes and F.G. Cuevas, *Metals*, **11**, 730 (2021); https://doi.org/10.3390/met11050730
37. T. Sun, L. Dong, C. Wang, W. Guo, L. Wang and T. Liang, *N. Carbon Mater.*, **28**, 349 (2013); https://doi.org/10.1016/S1872-5805(13)60087-6
38. V.L. Patil, S.A. Vanalakar, P.S. Patil and J.H. Kim, *Sens. Actuators B Chem.*, **239**, 1185 (2017); https://doi.org/10.1016/j.snb.2016.08.130
39. Y. Xu, L. Zheng, C. Yang, W. Zheng, X. Liu and J. Zhang, *ACS Appl. Mater. Interfaces*, **12**, 20704 (2020); https://doi.org/10.1021/acsami.0c04398
40. S. Kim, D.-H. Cho, H.-K. Chang, H.-N. Lee, H.-J. Kim, T.J. Park and Y.M. Park, *Sens. Actuators B Chem.*, **358**, 131486 (2022); https://doi.org/10.1016/j.snb.2022.131486
41. A.E. Mohajir, M.A.P. Yazdi, A. Krystianiak, O. Heintz, N. Martin, F. Berger and J.-B. Sanchez, *Chemosensors*, **10**, 426 (2022); https://doi.org/10.3390/chemosensors10100426
42. S. Das, S. Kumar, J. Singh and M. Kumar, *Sens. Actuators B Chem.*, **367**, 132114 (2022); https://doi.org/10.1016/j.snb.2022.132114
43. J.-B. Yu, M. Sun, M. Yu, M. Yang, H. Yu, Y. Yang, X.-T. Dong and L. Xia, *J. Alloys Compd.*, **920**, 165884 (2022); https://doi.org/10.1016/j.jallcom.2022.165884
44. L. Chen, H. Shi, C. Ye, X. Xia, Y. Li, C. Pan, Y. Song, J. Liu, H. Dong, D. Wang and X. Chen, *Sens. Actuators B Chem.*, **375**, 132864 (2023); https://doi.org/10.1016/j.snb.2022.132864